ISSUE: January 2025

Assessing Performance Of A 10-kW String Inverter Based On GaN FETs

by Riccardo Ruffo and Vedatroyee Ghosh, Texas Instruments, Freising, Germany

In the past few years, there has been an exponential increase of power going into the grid supplied by photovoltaic systems. These systems require more efficient solar inverters, which convert power from the dc panel into the 50- or 60-Hz ac carried by the grid. These inverters are typically referred to as string inverters since they convert power supplied by a string of series-connected solar panels.

Because photovoltaic systems stop generating energy when the sun goes down, many systems incorporate battery-based energy storage to guarantee the availability of power overnight or during a power outage. In such systems, an additional power conversion stage is required between the inverter and the battery pack to manage charging and discharging of the battery.

The implementation of wide-bandgap power devices based on gallium nitride (GaN) helps string inverters achieve lower switching losses. At the same time, they enable use of much smaller magnetic components thanks to a significant increase in switching frequency compared to silicon-based power devices.

In this article, we'll describe a low-cost 10-kW single-phase string inverter based on GaN power devices. The string inverter consists of two nonisolated power stages—a dc-dc converter comprised of two independent boost converters and a dc-ac converter. The design's high efficiency also enables you to connect a nonisolated dc-dc converter directly to an energy storage system (ESS), and to install it on the same heat sink with other power-conversion systems.

The article begins by discussing the design of the three power stages including the selection of their key components, operating parameters, and details of circuit operation. Interesting aspects of this design include the bidirectional operation of the dc-dc stage that manages power flow to and from the battery, the use of the HERIC topology in the dc-ac stage, and digital control of all three power stages using a single MCU.

Following the descriptions of the inverter design, experimental efficiency and thermal performance results are presented for each of the power stages over the expected range of operating conditions. The article concludes with some analysis of the measured performance.

Single-Phase String Inverter Design

Fig. 1 is a photograph of the 10-kW GaN-based single-phase string inverter with battery energy storage system (BESS) reference design from Texas Instruments (TI), including the heat sink. The design has a bidirectional power-conversion system for BESSs.

Fig. 1. A 10-kW single-phase reference design based on GaN.

Fig. 2 is a schematic representation of the system, which consists of two photovoltaic string inputs, each able to handle as many as 10 photovoltaic panels in series, and one ESS port that can handle battery stacks with voltages ranging from 50 V to 500 V. The nominal rated power from the string inputs to the BESS can reach 10 kW.

The bidirectional dc-ac converter can support up to 4.6 kW when connected to a single-phase grid at 230 V. In all of the power stages, we selected TI's LMG3522R030[1] top side-cooled GaN FETs to improve the heat transfer performance in this system. The total heat dissipation of the power devices is dissipated by a heat sink which is a static-cooled (fanless) solution.

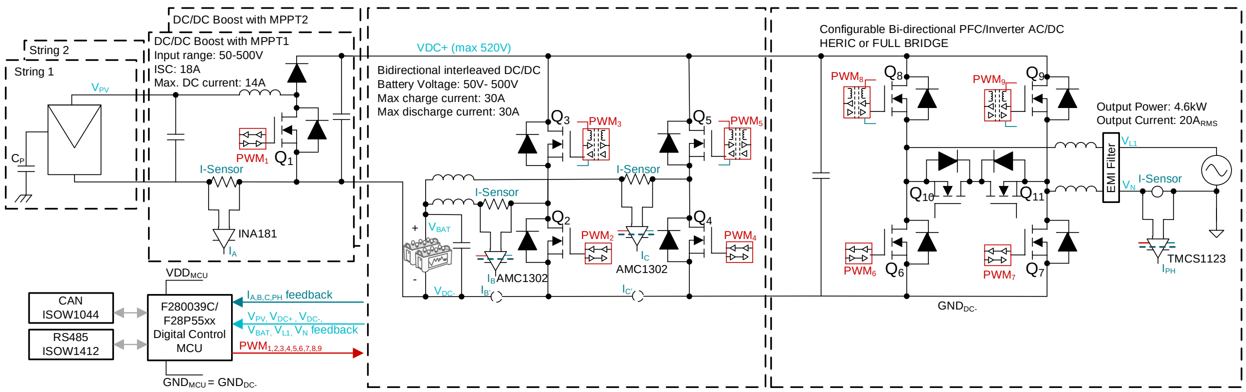

Fig. 2. Schematic representation of the 10-kW string inverter.

To address the cost sensitivities of the end equipment, one microcontroller (MCU) controls all of the power stages. Thanks to the integration of gate drivers in the GaN power devices, we can ground the MCU to the negative rail of the dc link, thus decreasing some of the requirements for isolation and power. The MCU controls all of the power stages at an equivalent interrupt service routine (ISR) of 20 kHz.

Boost Converter Stage

As you can see on the left side of Fig. 2, the boost converter stage constitutes two parallel independent string inputs with one common output rail (the dc link, which is labeled VDC+ (max 520 V) in Fig. 2). The output voltage of each string of photovoltaic panels is variable; various factors such as ambient temperature, irradiance (amount of sunlight) and the number of panels in series define and influence it. Each string output connects to a boost converter stage that boosts the string voltage output to an equal or higher voltage with respect to the dc link.

Based on the available current and voltage, the boost converter can operate in discontinuous conduction mode (DCM) or continuous conduction mode (CCM), but is always switching at a fixed 120-kHz frequency. This frequency is below the 150-kHz conducted emission mask, thus simplifying the electromagnetic interference (EMI) filter design. The boost converters can also handle string currents as high as 14 A, thus matching most of the nominal currents of panels available on the market.

In this stage, implementing the maximum power point tracking (MPPT) algorithm for each string will convert the maximum power available from the panels. To run the MPPT algorithm, the MCU reads and then controls the current and voltage of the string. The system does not need isolation between the controller and the power stages because the logic is referenced to the negative rail. We measure the string currents with a shunt-resistor, localized on the negative rail, together with a current-sense operational amplifier such as TI's INA181[2].

A current-sense amplifier was selected in this design instead of a standard op amp because the current-sense amplifier has an integrated precise, matched resistive gain network. This network enables robust current measurement across the whole specific temperature range and is less prone to noise. We measure the string voltage with a voltage divider, the output of which you can amplify before reaching the MCU.

Bidirectional DC-DC Converter

In cost-sensitive applications that entail charging and discharging a high-voltage battery, we recommend nonisolated topologies such as a bidirectional interleaved dc-dc boost converter.[3] On the central part of Fig. 2, you can see the two-phase interleaving stage implemented in this system.

The goal of this interleaving stage is to increase the charge and discharge current of the battery, thus allowing high-enough power conversion in a low-voltage battery pack. Each branch can handle up to 15 A, thus leading to a total charge and discharge current of 30 A. Each branch is switching in CCM at a switching frequency of 60 kHz with a dead time of 100 ns, leading to an equivalent frequency of the ripple current into the battery of 120 kHz.

As shown in Fig. 3, in order to control this stage, there are two independent current-control loops (proportional-integral controllers). Each current-control loop is responsible for controlling the single current of the half bridge, thus allowing a balanced current between the two half bridges. In order to accurately control the power drained and sourced from the battery, we implemented TI's shunt-based AMC1302[4] current-sensing isolated amplifier on the switching node, which allows precise and accurate measurements over high temperature variations in the system.

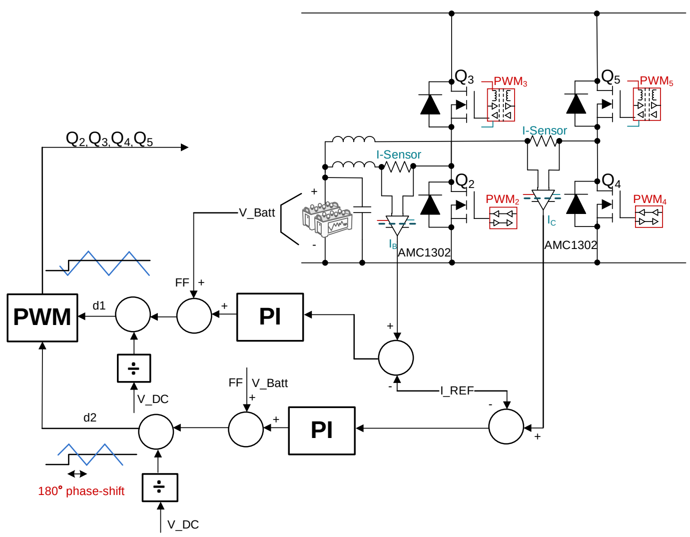

Fig. 3. Current-control loops implemented on the interleaved converter.

The battery pack always includes battery management systems that need to communicate with the power source. With the MCU referenced to the negative rail of the dc link, the system provides reinforced isolation between the string inverter and the battery pack communication unit through the use of two isolated transceivers: TI's ISOW1044[5] for controller area network (CAN) communication and TI's ISOW1412[6] for RS-485 communication.

DC-AC Converter

In a photovoltaic inverter, the inverter stage needs to be able to push power from the dc to the ac side. We selected a well-known topology in solar applications called the highly efficient and reliable inverter concept (HERIC) for the performance assessment. As shown on the right side of Fig. 2 (repeated below for the reader's convenience), the HERIC topology consists of an H-bridge, with each group of diagonal switches operating at a high frequency during one half wave of the grid voltage sine wave.

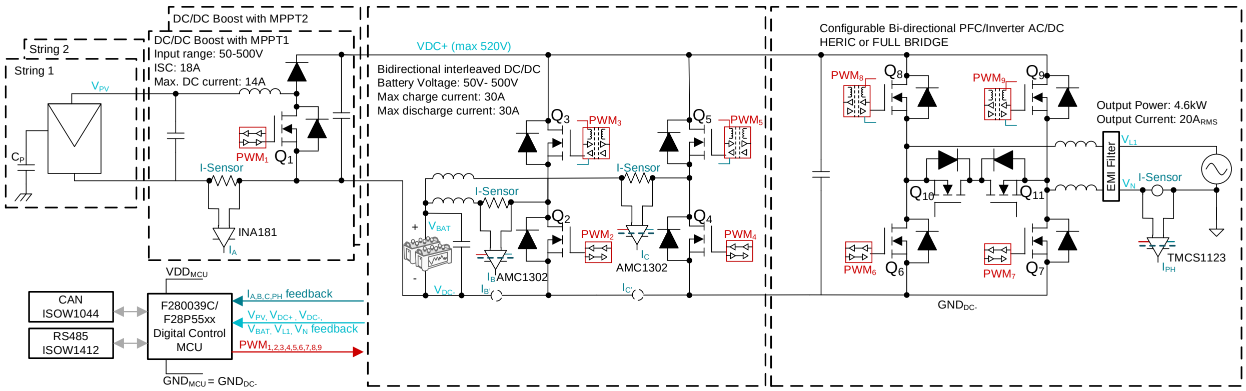

Fig. 2 again. Schematic representation of the 10-kW string inverter.

The HERIC topology allows the converter to apply three voltage levels on the output, thus making the differential filter smaller (Vdc+, Vdc–, zero). When the grid voltage is positive, the HERIC applies the Vdc+ and zero levels. When the voltage of the grid is negative, the HERIC applies the –Vdc and zero levels. From a common-mode noise perspective, the introduction of two additional switches reduces the common-mode noise applied by the converter quite significantly.

The HERIC topology is a good choice for transformerless string inverter applications where no isolation is available between the ac grid and the photovoltaic panels.[7] Leakage currents are a well-known challenge in photovoltaic applications given the vast photovoltaic surfaces exposed over grounded roofs or other surfaces. Such a large surface area can potentially lead to high values of stray capacitance between the photovoltaic panel and ground—values as high as 200 nF/kWpeak in damp environments or on rainy days.

The parasitic capacitance can then cause high common-mode current flowing into the system, affecting safety and causing unwanted triggering of residual current detection (RCD) devices. The system can achieve a common-mode voltage equal to zero by using the two additional power devices in the HERIC topology. Creating a short-circuit with Q10 and Q11 achieves disconnection from the dc link.

In the dc-ac stage of the targeted solar inverter, the switches are switching at a frequency of 85 kHz with a dead time of 150 ns. A series of proportional resonant controllers derives the duty cycles used to control the power devices, as shown in Fig. 4.

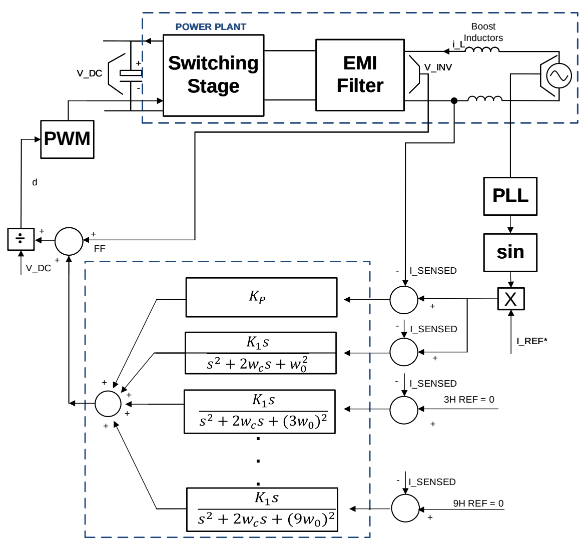

Fig. 4. Control of the dc-ac stage.

These proportional resonant controllers control the current to push power toward the grid at the fundamental frequency, and attenuate the higher orders of harmonics to the zero level in order to improve the total harmonic distortion. A second-order generalized integrator single-phase phase-locked loop derives the fundamental frequency.

In Fig. 4, you can control the current either at the point of common coupling (PCC) or on the switching node. In this design, the TMCS1123[8] high-bandwidth Hall-effect current sensor (shown in Fig. 2) controls the current on the PCC, thus enabling an improved power factor when pushing power toward the grid.[9]

Experimental Results

Fig. 5 depicts the efficiency of one input dc-dc boost converter when regulating the dc link at 400 Vdc at the 120-kHz fixed switching frequency. You can measure the efficiency from the string inverter to the dc link by keeping the string voltage constant (50 V, 150 V, 200 V, 250 V and 350 V) and changing the current.

Fig. 5 shows that while it is possible to achieve a peak efficiency of 99.3% at full load, applying 50-V results in a 3.5% efficiency drop. This is happening because the switching and conduction losses are still there, but there is a significant decrease in the power transfer. Implementing variable-frequency control can improve efficiency >1%, when 50 V is applied on the input.

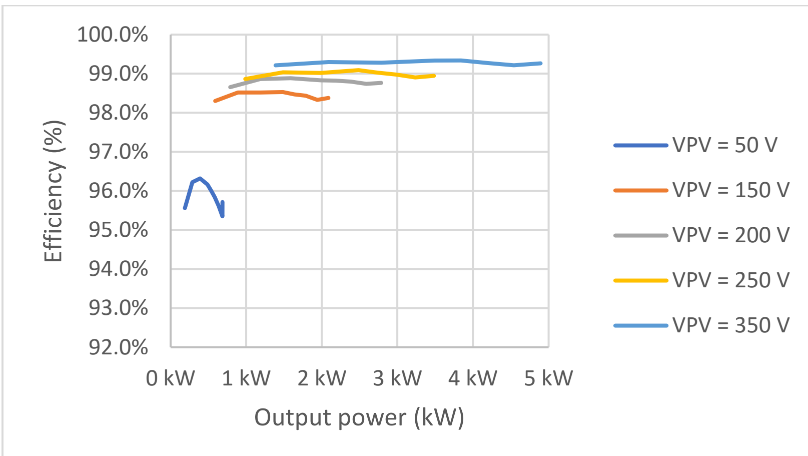

Fig. 5. Efficiencies at different load points of the boost converter control when applying 400 V on the dc bus.

An important feature of the LMG3522R030 FET is the option to read out the junction temperature. This enables easy and efficient temperature monitoring of the system directly at the points of interest. Fig. 6 shows the temperature rise of the GaN FET for the worst-case duty-cycle operation: conversion of a 50-V input to a dc bus voltage of 400 V.

Notice that the temperature rise does not exceed 35°C even though it is a static-cooled operation. Fig. 6 also highlights the temperature rise of the silicon carbide diode for an operation corresponding to its worst-case duty-cycle: a 350-V conversion to 400 V on the dc link.

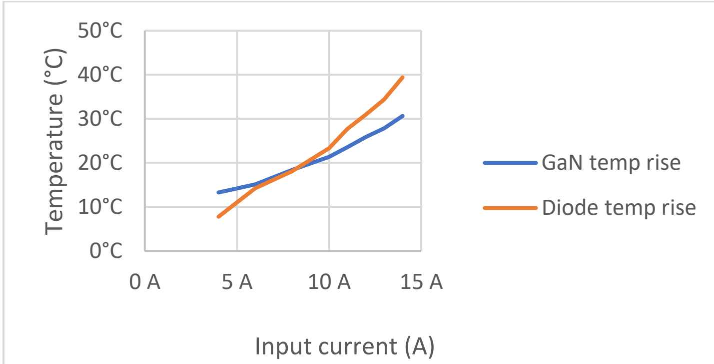

Fig. 6. Diode and GaN junction temperature rise for worst-case duty-cycle operation of the bidirectional dc-dc converter.

Fig. 7 shows the efficiency of the interleaving dc-dc converter charging battery packs with different voltage levels when having 400 V on the dc link. The input battery voltages are 80 V, 160 V, 240 V and 320 V. You can see that, when the converter is charging, it is always presenting higher efficiency when charging a high-voltage battery pack, as 320 V. There is a significant drop in efficiency, especially at lower power and lower voltages. We recommend applying the phase-shedding technique when the power requested is less than half the nominal power.

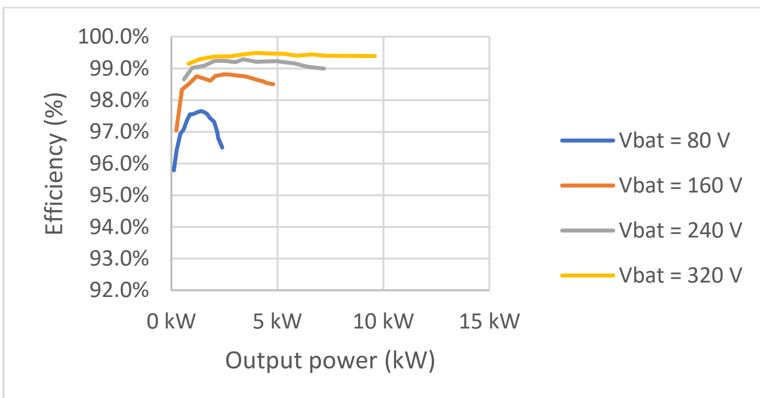

Fig. 7. Efficiencies at different load points of the bidirectional dc-dc converter in boost mode.

Fig. 8 shows the junction temperature of the hottest device in the converter when in boost mode.

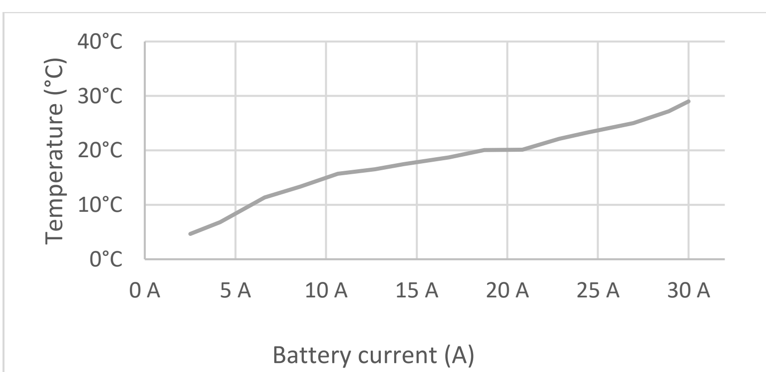

Fig. 8. GaN junction temperature rise of the bidirectional dc-dc converter in boost mode.

As shown in Fig. 9, the dc-ac converter based on GaN achieves a peak efficiency of 98.5% at a half load and 400-V input, and 98.2% at a full load. This efficiency includes all of the power dissipated by the auxiliary power supplies.

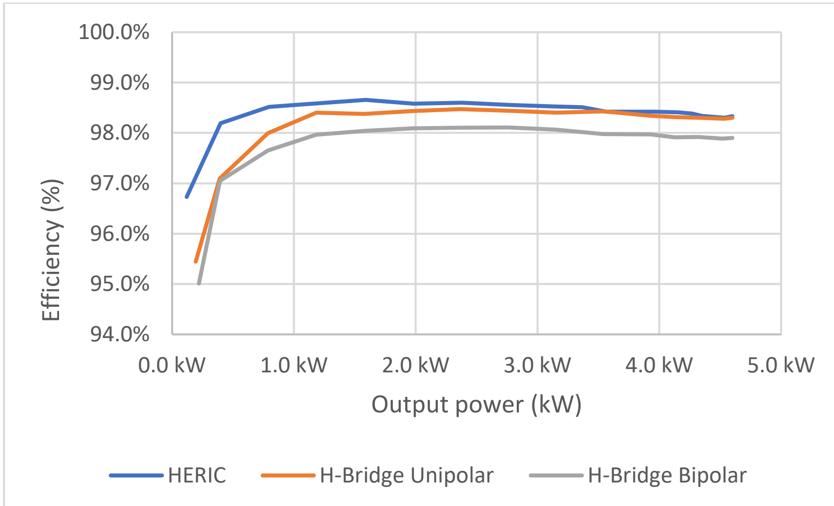

Fig. 9. Efficiencies at different load points of the dc-ac converter.

In order to understand how the HERIC converter is performing with respect to a standard H-bridge topology, we disabled GaN devices Q10 and Q11 and ran the H-bridge using the bipolar and unipolar modulation schemes. As you can see in Fig. 9, the efficiency of the HERIC is always higher than a standard H-bridge converter, particularly at light loads.

This is because the devices in a HERIC converter, especially at light loads, are turning on with a voltage equivalent to half the dc link. This leads to an important reduction in the losses caused by the parasitic drain-to-source capacitance (C_{OSS}). On the other hand, you can also see that the bipolar topology is much less efficient; the conduction losses are higher given the two-level nature of the ripple.

Fig. 10 shows sourcing of around 4.4-kW output power from a 400-Vdc link to 230 Vac, with the line voltage in yellow and the line current in pink. The total harmonic distortion of the current is negligible. Fig. 10 also shows the dc link power ripple present at 100 Hz in green.

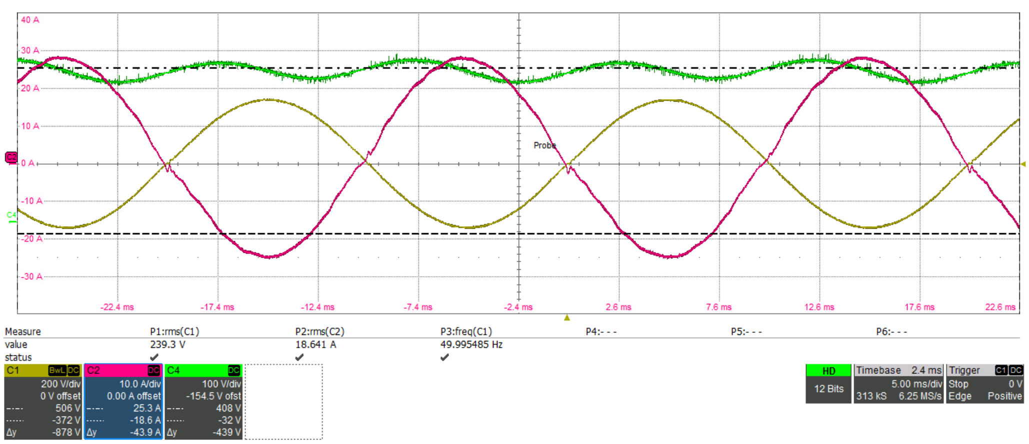

Fig. 10. Grid current (pink trace), grid voltage (yellow trace) and dc bus voltage waveforms.

Fig. 11 shows the junction temperature of the hottest device. Even at a full load, the temperature does not rise higher than 20°C, thus showing that the losses are low.

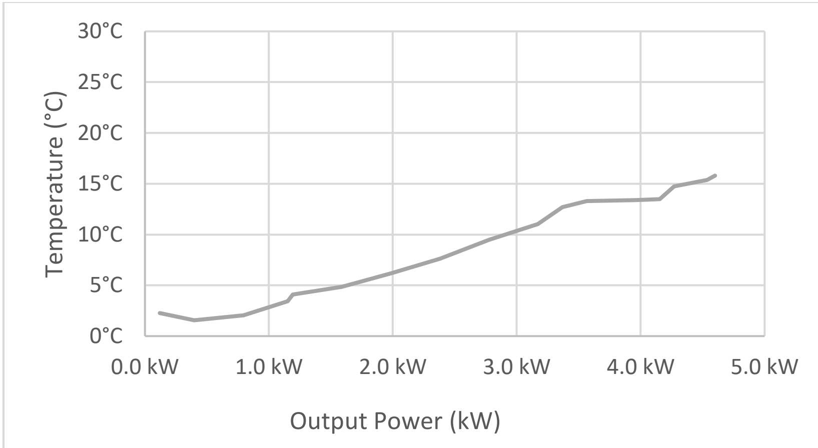

Fig. 11. GaN junction temperature rise of the dc-ac converter.

Conclusion

In this article, we assessed the performance of a string inverter based on GaN technology. The introduction of GaN devices enables the converter to switch much faster, but still keeps the same order-of-magnitude efficiency as a silicon solution.

We have observed that the switching frequency could be increased by a factor higher than 6x with respect to state-of-the-art IGBT-based string inverters. This leads to a reduction in volume and weight of the passive components of up to four times.

Even at high power and high switching frequencies, the performance is good. The higher switching frequency leads to an important reduction in filter dimensions, thereby increasing the power density, which could become an important factor when designing residential photovoltaic inverters. TI's 10-kW GaN-based single-phase string inverter with battery energy storage system reference design[10] includes ready-to-use system files to speed your design process, as well as software support.

References

1. LMG3522R030 product page.
2. INA181 26-V bidirectional 350-kHz current-sense amplifier product page.
3. "Sensorless Control of the Charging Process of a Dynamic Inductive Power Transfer System with an Interleaved Nine-Phase Boost Converter" by Riccardo Ruffo, Vincenzo Cirimele, Michela Diana, Mojtaba Khalilian, Alessandro La Ganga and Paolo Guglielmi, IEEE Transactions on Industrial Electronics 65, no. 10 (October 2018): pp. 7630-7639.
4. AMC1302 precision current sensing reinforced isolated amplifier product page.
5. ISOW1044 isolated CAN FD transceiver with integrated dc-dc power product page.
6. ISOW1412 reinforced isolated RS-485/RS-422 transceiver with integrated power product page.
7. "Comparison of AC/DC Power-Conversion Topologies for Three-Phase Industrial Systems" by Ricardo Ruffo, Kelvin Le and Harald Parzhuber, Texas Instruments Power Supply Design Seminar SEM2600, literature No. SLUP417, 2024-2025.
8. TMCS1123 reinforced isolation, 80-Arms, 250-kHz Hall-effect current sensor product page.
9. "Design Considerations for Current Sensing in DC EV Charging Applications" by Riccardo Ruffo, Lei Song and Harald Parzhuber, Texas Instruments, literature No. SBAA541.
10. "10-kW GaN-based single-phase string inverter with battery energy storage system," TI reference design TIDA-010938.

About The Authors

Riccardo Ruffo, who has been at Texas Instruments Germany since 2021, works as a system engineer in the Energy Infrastructure sector. His main work includes EV charging, inductive wireless power transfer, photovoltaic, renewable energy, and energy storage applications. Ruffo Riccardo received the Ph.D. degree in electric, electronics and communication engineering from Politecnico di Torino, Turin, Italy.

Vedatroyee Ghosh is a systems engineer at Texas Instruments Germany in the Energy Infrastructure team where she focuses on photovoltaics, power conversion systems, and energy storage systems. Vedatroyee has earned her master's degree in power engineering from the Technical University of Munich, Germany.

For further reading on solar inverter design, see the "How2Power Design Guide," locate the Popular Topics category and select "Solar Power Inverters".